# JL 82: a slowly pulsating hot subdwarf star in a close binary system

C. Koen[*]

*Department of Statistics, University of the Western Cape, Private Bag X17, Bellville, 7535 Cape, South Africa*

**ABSTRACT**

JL 82 is a known binary, consisting of an sdB star and a companion which is not directly observable in the optical. Photometric measurements reported in this paper show it to variable with both the binary period (∼0.75 d), as well as on much shorter time-scales. The shorter periods are ascribed to pulsation of the sdB star, making it a member of the PG 1716 class of pulsating stars.

**Key words:** binaries: close – stars: individual: JL 82 – stars: oscillations – subdwarfs – stars: variables: other.

## 1 INTRODUCTION

The designation 'JL' indicates that the subject of this paper was first identified by Jaidee & Lynga (1974) as a very blue object. It was subsequently recovered in the Edinburgh–Cape faint blue object survey (Kilkenny et al. 1995), and catalogued as EC 21313−7301. The latter paper showed a spectrum of the star, and assigned the classification as a B-type subdwarf. The effective temperature and gravity of the sdB star have been estimated at $T_{\text{eff}} = 25\,000$ K and $\log g = 5.0$, respectively (Edelmann 2003).

JL 82 is a Landolt standard star; the optical photometric indices are $V = 13.389$, $B - V = -0.208$, $U - B = -0.947$, $V - R = -0.098$, $V - I = -0.211$ from 21 measurements over 11 nights (Landolt 2007). It is very useful for present purposes that Landolt (2007) selected four other stars in the field of JL 82 as additional standards: the measured magnitudes of two of these, JL 82B ($V = 13.507$, $B = 14.212$, $I = 12.682$) and JL 82C ($V = 13.440$, $B = 14.052$, $I = 14.155$) were used to standardize the photometry reported below. Near-infrared photometry [$J = 12.86$ (0.024), $H = 12.96$ (0.025) and $K_S = 13.05$ (0.037)] is available from the Two-Micron All-Sky Survey catalogue (Skrutskie et al. 2006).

Radial velocity measurements by Edelmann et al. (2005) revealed JL 82 to be a single-lined spectroscopic binary, with a period of 0.7371 (5) d [$f = 1.3567$ (9) d$^{-1}$]. A lower limit of $0.1\,M_{\odot}$ could be placed on the companion mass: according to Edelmann et al. (2005), likely companions to the sdB star are a low-mass main-sequence star, or perhaps a white dwarf.

It is of interest to consider whether the infrared photometry reveals the presence of a cool companion. Stark & Wade (2003) and Reed & Stiening (2004) have addressed, in general, this point for sdB stars. The two sets of colour indices [$(B - V) = -0.21$, $(J - K_S) = -0.19$] and [$(V - K_S) = -0.66$, $(J - K_S) = -0.19$] place JL 82 firmly amongst the single sdB stars in fig. 1 of Stark & Wade (2003). Similarly, the indices $(J - H) = -0.10$, $(H - K_S) =$

−0.09, $(J - K_S) = -0.19$ and $(B - J) = -0.68$ indicate that any main-sequence companion to the sdB star should be of later type than M2, according to fig. 1 in Reed & Stiening (2004).

The lower limit of $0.1\,M_{\odot}$ derived by Edelmann et al. (2005) for the secondary star mass rules out a brown dwarf companion. The reflection effect reported below excludes any hot secondary: it is therefore concluded that the unseen component of the binary is an M dwarf, with mass in the approximate range 0.1–$0.4\,M_{\odot}$.

This paper describes the results of several photometric observation runs on JL 82, which led to the discovery that it is not only a reflection effect binary, but also that the hot subdwarf star pulsates. The experimental work is described in Section 2, and the analysis of the data in Sections 3 and 4. The results are discussed in Section 5.

## 2 THE OBSERVATIONS

All measurements were made with the South African Astronomical Observatory (SAAO) STE4 CCD camera mounted on the SAAO 1.0-m telescope at Sutherland, South Africa. The field of view of the camera on the telescope is $5 \times 5$ arcmin$^2$. Pre-binning of the images was performed throughout, giving a reasonable readout time of about 17 sec. Observations were cycled through the $B$, $V$ and $I_C$ filters – see Table 1 for an observing log.

Photometric reductions were performed using an automated version of DOPHOT (Schechter, Mateo & Saha 1993). Profile-fitted magnitudes were used – the scatter in these was usually marginally smaller than in the aperture photometry. Differential measurements with respect to two of the three brightest stars in the field of view, JL 82B and JL 82C (Landolt 2007), were calculated (JL 82A was too bright). Nightly zero-points were set by the mean magnitude of the two local comparison stars.

The results are plotted in Figs 1 ($B$), S1 ($V$) and S2 ($I_C$) (see Supporting Information). There are obviously two time-scales of variability: one of about 0.05 d (roughly an hour), the other longer than the longest of the runs (i.e. longer than 8 h). Another view of this information is presented in Fig. 2, in which the amplitude spectra of the three data sets are plotted. Concentrations of power around

[*]E-mail: ckoen@uwc.ac.za

**Table 1.** The observing log. Much of the observing was done through thin cirrus, which required adjustment of the exposure time $T_{exp}$. The minimum number of useful measurements in any filter obtained during each night is given in the last column.

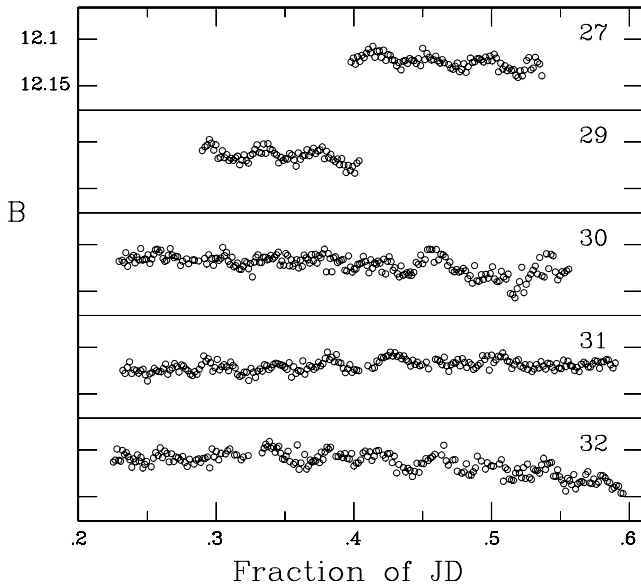| Starting time (HJD 2454700+) | $B$ | $T_{exp}$ (s) $V$ | $I_C$ | Run length (h) | $N$ |
|---|---|---|---|---|---|
| 27.3981 | 30–40 | 15–20 | 30–50 | 3.0 | 85 |
| 29.2899 | 30–40 | 15–25 | 30–40 | 2.4 | 72 |
| 30.2297 | 20–30 | 15–20 | 20–30 | 7.5 | 221 |
| 31.2323 | 30 | 20 | 30 | 8.2 | 213 |
| 32.2254 | 20–30 | 15–20 | 20–30 | 8.5 | 220 |



**Figure 1.** Light curves obtained in the $B$ band. The vertical width of each panel is 0.11 mag. Panels are labelled with the last two digits of the Julian day of observation.
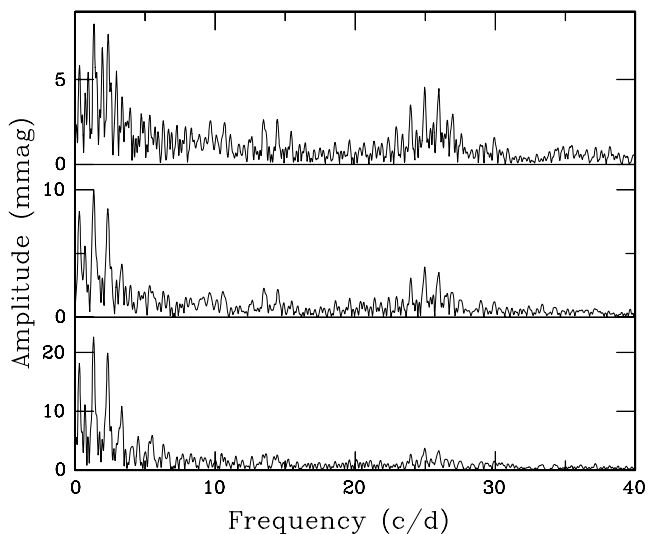


**Figure 2.** Amplitude spectra of the data sets in Figs 1, S1 and S2. From top to bottom panel: $B$, $V$ and $I$. Note the different scales on the vertical axes of the three panels.

2, 14 and 25 $d^{-1}$ are clearly visible. The amplitudes of the two higher frequency power excesses decrease with increasing wavelength; the reverse applies to the low-frequency variations.

Pre-whitening the data by a low-order polynomial removes variations with frequencies below about 4 $d^{-1}$. The remaining higher frequency content is discussed in the next section of the paper, while Section 4 deals with the low-frequency variations.

## 3 THE SHORTER TIMESCALE VARIABILITY

The rapid variations are easily extracted by pre-whitening the individual light curves by second-order polynomials. Nightly amplitude spectra for each of the three filters are plotted in Figs 3–5. Inspection of the figures shows the following.
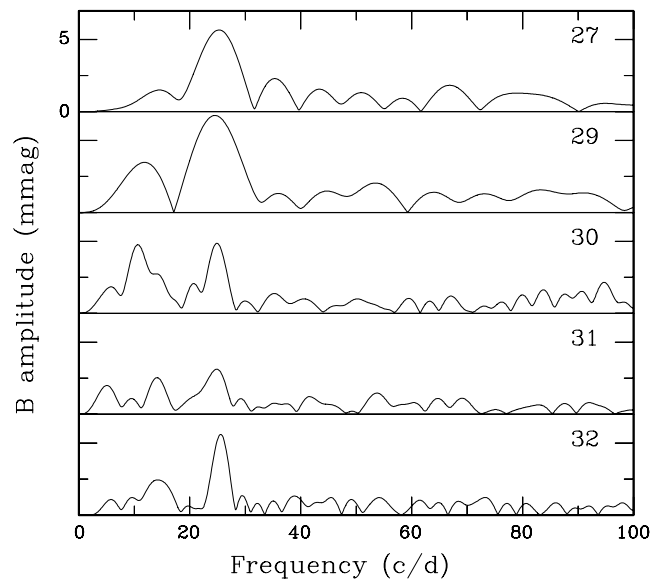


**Figure 3.** Amplitude spectra of the high-frequency $B$-band data. Panels are labelled with the last two digits of the Julian day of observation.
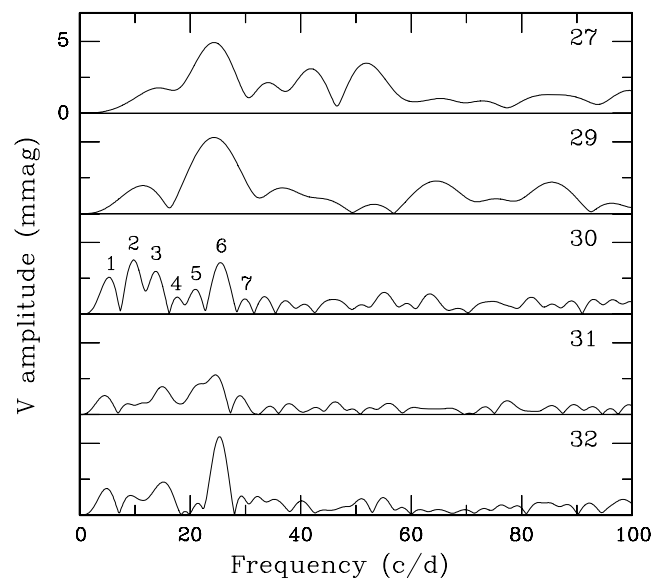


**Figure 4.** Amplitude spectra of the high-frequency $V$-band data. Panels are labelled with the last two digits of the Julian day of observation.
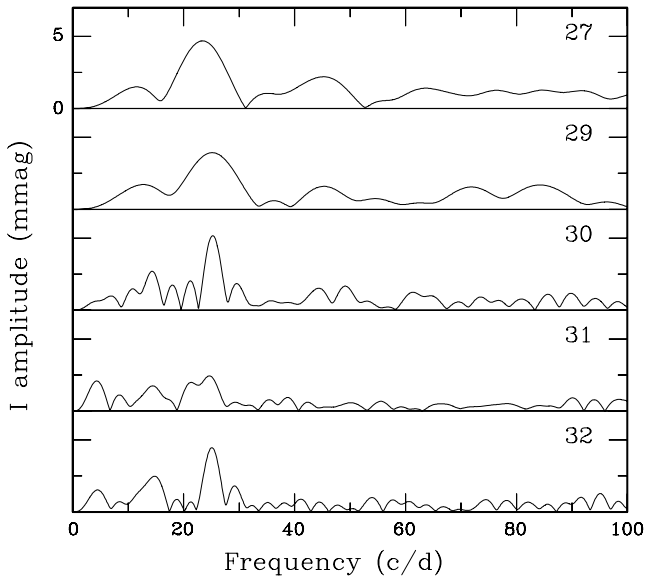
**Figure 5.** Amplitude spectra of the high-frequency $I_C$-band data. Panels are labelled with the last two digits of the Julian day of observation.

(i) Recurring features are restricted to frequencies below about $35\ \mathrm{d}^{-1}$.

(ii) For a given night, peaks in the spectra appear at roughly the same frequencies in the data for the different filters.

(iii) There is considerable variation in the shape of the spectra from night to night – see particularly the spectra in the bottom three panels (which correspond to the three longest observing runs).

(iv) A close look at the spectra for the last three nights none the less suggests that peaks recur at the seven frequencies marked in the middle panel of Fig. 4. The recurrences are both night-to-night and filter-to-filter.

(v) The amplitude of a peak at a given frequency varies from night-to-night – see, e.g., the principal peak near $25\ \mathrm{d}^{-1}$ (marked '6' in Fig. 4).

(vi) At a given frequency, the ranking of the amplitudes amongst the three filters can change from one night to another. As an example, compare the heights of the principal peaks on HJD 2454730 and HJD 2454732: the ranking changes from $I - B - V$ to $B - V - I$. Assuming the same frequency content is to be seen in all filters, this suggests that the phases are not the same in the different wavebands.

For each of the three filters, the nightly detrended data were next combined, and frequencies extracted. The procedure followed was: (i) calculate the amplitude spectrum of the data over the frequency interval $0 < f < 35\ \mathrm{d}^{-1}$ (suggested by Figs 2–5); (ii) note the frequency $f_1$ at which the spectrum reaches an overall maximum; (iii) using linear least squares, fit a sinusoid with frequency $f_1$ to the data; (iv) subtract the fitted sinusoid from the data (i.e. 'pre-whiten' the data by $f_1$) and (v) repeat steps (i)–(iv) on the pre-whitened data until it appears that all 'signals' have been extracted from the data.

An illustrative example of pre-whitened spectra can be seen in Fig. 6, while the extracted frequencies are in Table 2. The following remarks can be offered.

(i) Only the two largest amplitude modes can be firmly identified in all three data sets: equating frequencies found in the different filters for all other modes is tentative, based on likely aliases.

(ii) It is possible that the second frequency is an aliased subharmonic of the first frequency.
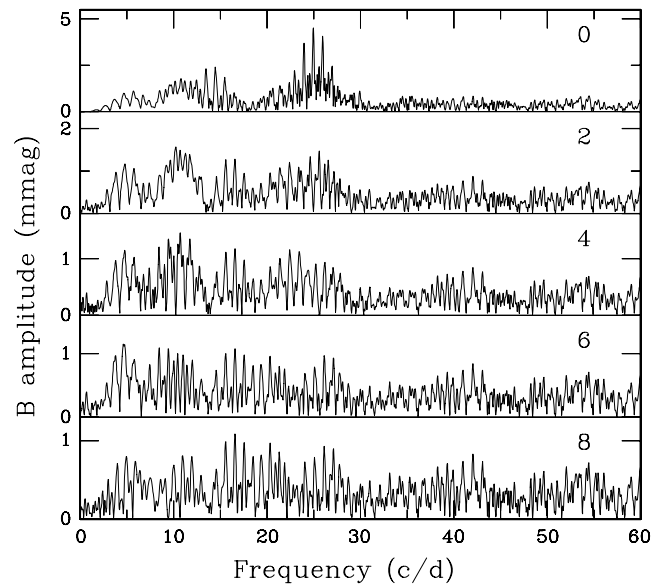


**Figure 6.** Amplitude spectra calculated for successive stages of pre-whitening of the *B*-band data. Panels are labelled with the number of pre-whitened frequencies. The order in which frequencies have been pre-whitened is the same as the frequency order in the *B*-band column in Table 4: for example, the third panel shows the spectrum after removal of 24.965, 13.47, 10.24 and 25.59 d⁻¹. Note the different vertical scales of the different panels.

**Table 2.** An inventory of amplitude spectrum peaks in the range $0 < f < 35\ \mathrm{d}^{-1}$, for each of the three data sets.

| Frequency (d⁻¹) | | | Amplitude (mmag) | | |
| --- | --- | --- | --- | --- | --- |
| *B* | *V* | *I* | *B* | *V* | *I* |
| 24.965 (7) | 24.972 (7) | 24.963 (6) | 4.5 (3) | 3.9 (3) | 4.0 (2) |
| 13.47 (1) | 14.50 (1) | 14.47 (1) | 2.3 (3) | 1.9 (3) | 1.9 (2) |
| 10.24 (2) | 10.13 (2) | 11.34 (2) | 1.6 (3) | 1.0 (2) | 1.0 (2) |
| 25.59 (2) | 26.46 (2) | 25.49 (2) | 1.5 (3) | 1.1 (2) | 1.1 (2) |
| 10.71 (2) | | | 1.5 (3) | | |
| 23.47 (2) | 21.39 (2) | 21.36 (2) | 1.2 (3) | 1.4 (2) | 1.1 (2) |
| 4.62 (2) | 4.56 (2) | 4.35 (2) | 1.1 (3) | 1.1 (2) | 1.3 (2) |
| 9.43 (2) | 9.56 (2) | 9.57 (4) | 1.1 (3) | 1.3 (2) | 0.6 (2) |
| 16.57 (2) | 16.64 (3) | | 1.0 (2) | 0.9 (2) | |
| 26.14 (3) | 25.22 (3) | 24.13 (3) | 0.9 (3) | 0.9 (2) | 0.7 (2) |
| 21.29 (3) | | 21.10 (3) | 0.9 (2) | | 0.7 (2) |
| 11.03 (3) | 11.92 (3) | | 0.9 (3) | 0.9 (2) | |
| 4.96 (3) | 5.02 (2) | 4.73 (4) | 0.8 (2) | 1.3 (2) | 0.6 (2) |

(iii) If, for example, the frequencies 25.59, 26.46 (alias of 25.46?) and 25.49 d⁻¹ all refer to the same mode, then the formal frequency errors ($\sim 0.02$) are severe underestimates.

(iv) It is curious that there are not even tentative counterparts in the *V* and *I* data for the 10.71 d⁻¹ mode found in the *B*-band data.

(v) For the four highest amplitude modes, the *B*-band amplitudes are consistently higher than those seen in *V* and *I*; the *V* and *I* amplitudes are essentially equal.

(vi) The lowest frequencies (around 4.6 d⁻¹) are again found in the analysis reported in Section 4 (see Table 3). The amplitudes in Table 2 are considerably lower, which is to be expected given the filtering of low-frequency power. It is noteworthy that the *B* and *V*

**Table 3.** Low frequencies extracted from the data by successive pre-whitening.

| | Frequency (d$^{-1}$) | | | Amplitude (mmag) | |
|---|---|---|---|---|---|
| *B* | *V* | *I* | *B* | *V* | *I* |
| 1.346 (6) | 1.328 (4) | 1.326 (2) | 6.1 (3) | 7.8 (3) | 17.7 (3) |
| | 1.650 (8) | 1.659 (8) | | 3.3 (3) | 3.6 (3) |
| 3.48 (2) | 4.47 (1) | 3.460 (7) | 2.7 (3) | 2.5 (2) | 4.4 (3) |
| 1.935 (9) | | | 3.4 (3) | | |

amplitudes of this mode are similar, while the *I*-band amplitude is larger.

It would obviously be useful to have some idea of the statistical significance levels of the entries in Table 2, but it is not clear how these could be calculated. There are, of course, the usual problems posed by periodograms – particularly issues with non-white noise, aliasing, the presence of multiple signals and the erosion of significance levels by multiple hypothesis testing. In this paper, the identification of possibly important frequencies is based primarily on their recurrence in the data from different filters. This seems a reasonable approach to take, but the author is not aware of any study which deals with significance levels of the results. This is perhaps not surprising, because, in addition to the problems posed by the interpretation of ordinary periodograms, there are additional difficulties such as the slightly different aliases in the different data sets, and the effects of the (largely unknown) uncertainties in the frequencies extracted from the data for the different filters. It also seems that a formal approach should make use of the relative amplitudes expected for the signals seen through different filters. The results presented in this paper should therefore be seen as tentative. The author has chosen to err on the side of including too much, rather than too little, in order to provide as much information as possible for comparison with more extensive studies.

Standard procedure involves a further step in which the frequency set extracted by successive pre-whitening, is used as a basis for further iteration in simultaneous non-linear least-squares fitting of *all* frequencies, amplitudes and phases. The author does not deem the quality of the current data sufficient for this to be meaningful.

## 4 THE LONGER TIMESCALE VARIABILITY

Fig. 7 gives a finer resolution view of the low-frequency sections of the amplitude spectra in Fig. 2. Three sets of aliases are visible in the spectra; these are at roughly (0.31, 1.33, 2.34), (0.72, 1.75, 2.78) and (0.93, 1.95, 2.99) d$^{-1}$ in the case of the *I*-band data. The most prominent feature evidently corresponds to the spectroscopically determined binary period 0.7371 (5) d (i.e. $f = 1.3567$ (9) d$^{-1}$; Edelmann et al. 2005). The frequencies near multiples of 1 d$^{-1}$ could perhaps be due to slight mismatches in the nightly zero-points – note that these are much more prominent in the *B* band, which is considerably more susceptible to the effects of differential extinction (remember that JL 82 is much bluer than the comparison stars). A possible origin for the remaining set of frequencies is the first harmonic $f = 2.71$ d$^{-1}$ of the binary frequency.

It seems prudent to first pre-whiten frequencies above 6 d$^{-1}$ or so from the observations, particularly in the case of the *B* band. Once this has been done, successive pre-whitening gives the results in Table 3. As may have been anticipated from the light curves in Figs 1, S1 and S2, the amplitude of the binary variation increases with increasing wavelength. The 1.65 d$^{-1}$ frequency can now with
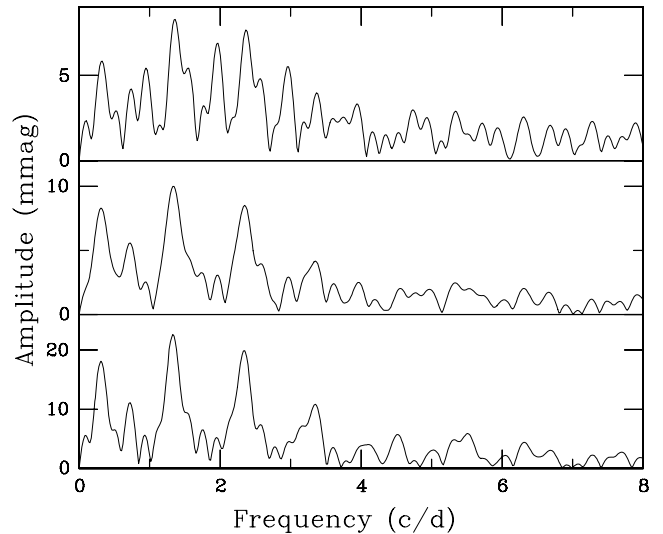


**Figure 7.** Low-frequency detail of the amplitude spectra in Fig. 2. From top to bottom panel: *B*, *V* and *I*. Note the different scales on the vertical axes of the three panels.

greater confidence (than 1.75 d$^{-1}$ found above) be identified as an alias of twice the binary frequency of 1.33 d$^{-1}$. Comparison with Table 2 also shows that the lowest frequencies there may have been recovered as the highest frequencies in Table 3.

Since the amplitude in the *I* band is much larger, and the *I*- and *V*-band frequencies very similar, $f = 1.326$ d$^{-1}$ ($P = 0.7541$d) is adopted as the most reliable estimate for the binary frequency. In Fig. S3, the data are shown phased with respect to this frequency.

## 5 DISCUSSION

### 5.1 The rapid variations

The most likely explanation for the short-period variations is pulsation of the sdB star. There are two classes of pulsating sdB stars: the rapidly pulsating EC 14026 stars with periods in the range 2–9 min (e.g. Kilkenny 2007) and the slowly pulsating PG 1716 stars with periods typically 1–2 h (e.g. Fontaine et al. 2006). The effective temperature of 25 000 and gravity log $g = 5$ determined by Edelmann (2003), and the range of periods in Table 2, place JL 82 amongst the latter group of stars.

JL 82 is the 10th PG 1716 star for which pulsation frequencies appear in print – its predecessors are PG 1716+426 (Green et al. 2003; Reed et al. 2004), Balloon 090100001 (Oreiro et al. 2004; Baran et al. 2005; Baran, Pigulski & O'Toole 2008), PG 0101+039 (Randall et al. 2006a), PG 1627+017 (Randall et al. 2006b), PG 1338+481 (Randall et al. 2006c), HS 0702+6043 (Schuh et al. 2006; Lutz et al. 2008), EC 21324−1346 (Kilkenny et al. 2007), KPD 0629−0016 (Koen & Green 2007) and HS 2201+2610 (Lutz et al. 2008). The frequencies observed in each of these stars are summarized in Table 4. (Further analyses, followed by time-resolved observations, have shown the slow pulsations claimed for HE 0230−4323 by Koen 2007 to have been aliases of rapid pulsations. This star is therefore not included in Table 4).

Inspection of the table shows that aside from JL 82, frequencies below 10 d$^{-1}$ (periods longer than 2.4 h) have only been found in PG 1627+017 (9.7 d$^{-1}$) and PG 1338+481 (9.1 d$^{-1}$). There are several possible reasons why periods longer than 3 h have only been

**Table 4.** Frequencies seen in the PG 1716 stars; see the text for references. All frequencies are listed if three or fewer have been found, otherwise the range of values is quoted. In the case of the hybrid EC 14026/PG 1716 stars (Bal 09, HS 0702+6043 and HS 2201+2610), only the lower PG 1716 like frequencies are considered.

| Star | Number of frequencies | Range ( $d^{-1}$ ) |
|---|---|---|
| PG 1716+426 | 6 | 15.8 – 29.4 |
| Balloon 090100001 | 4 | 20.7 – 31.6 (photometric) |
| | 6 | 14.6 – 40.1 (spectroscopic) |
| PG 0101+039 | 3 | 11.9, 16.5, 32.6 |
| PG 1627+017 | 23 | 9.7 – 18.9 |
| PG 1338+481 | 13 | 9.1 – 40.7 |
| HS 0702+6043 | 3 | 17.8, 23.5, 27.5 |
| EC 21324-1346 | 9 | 11.1 – 28.8 |
| KPD 0629−0016 | 5 | 12.3 – 31.4 |
| HS 2201+2610 | 1 | 26.5 |
| JL 82 | >10(?) | 5 (?) – 25 (?) |

found in JL 82: (i) these long periods are due to unmodelled aspects of the binary (reflection effect) variability, (ii) the long periods are due to uncorrected differential extinction, (iii) the periods are real pulsation periods, but rare, (iv) such long periods are also present in observations of other PG 1716 stars, but have been undetected due to the data analysis procedures (e.g. trend removal).

As far as JL 82 is concerned, the first explanation seems unlikely. The only apparent connection between the $\sim$4.5 $d^{-1}$ period in Tables 2 and 3 and the binary frequency of 1.34 $d^{-1}$ seems to be via a 1 cycle $d^{-1}$ alias of the fourth harmonic at 5.36 $d^{-1}$, but this is doubtful in the absence of good evidence for the presence of the third harmonic. Differential extinction also appears an unlikely culprit, as the amplitudes of the low-frequency features do not increase with decreasing wavelength of the observations. The author favours explanation (iv), since it is common practice to filter out frequencies in period intervals in which no variability is expected.

It would be interesting to see whether the long periods in JL 82 are spectroscopically detectable. However, this could only be used to confirm that these variations are intrinsic to the star, and not to disprove their existence: this follows because not all modes which are photometrically visible are necessarily spectroscopically detectable (e.g. Baran et al. 2008).

It is perhaps worth noting that the amplitude of the most prominent periodicity in Table 2 is amongst the largest seen in any of the PG 1716 stars. It also appears to have a particularly rich mode spectrum.

## 5.2 The slow variations

The most reasonable explanation for the photometric variability on the binary time-scale is that it is due to a reflection effect. Since the amplitude of the reflection effect increases with increasing wavelength, being largest in the *I* band, it may be concluded that the illuminated area on the otherwise unseen companion star is relatively cool. This indicates a red dwarf secondary star.

A number of attributes of the binary components can be deduced. It was mentioned in Section 1 that there is a lower limit of 0.1 $M_\odot$ on the secondary mass, and it was also deduced that the spectral type is M2 or later. Using fundamental properties of M dwarfs given in Reid & Hawley (2000; table 4.1), the following limits can be set: spectral type M2–M6, mass $M_2 = 0.44$–$0.1\,M_\odot$, radius 0.44–0.15 $R_\odot$ and $T_{\rm eff}$ in the range 3400–2600 K. Since $\log g = 5$ for the primary (Edelmann 2003), $R_1 = 0.37\,R_\odot$ for the canonical sdB mass $M_1 = 0.5\,M_\odot$.

It is interesting to consider whether there is consistency between these physical parameters and the low-frequency amplitudes measured through the different filters. For a given filter, the expected peak-to-peak amplitude is roughly given by

$$\Delta m \approx -2.5 \left[ \log \left( R_1^2 F_1 + R_2^2 F_h \right) - \log \left( R_1^2 F_1 + R_2^2 F_2 \right) \right], \quad (1)$$

where $F_1$, $F_2$, $F_h$ are, respectively, the blackbody fluxes from the subdwarf, the cool (unheated) hemisphere of the M dwarf and the heated hemisphere of the M dwarf. For the subdwarf, adopted parameters are a temperature $T_1 = 25\,000$ K and radius $R_1 = 0.37\,R_\odot$. The remaining unknowns, namely the radius $R_2$ and temperature $T_2$ of the secondary and the temperature $T_h$ of the heated hemisphere, can be obtained by fitting the three predicted amplitudes to the observed values.

The latter task is performed as follows: (i) assume a value for $T_2$, (ii) minimize

$$SS = [\Delta m(B, \text{observed}) - \Delta m(B, \text{predicted})]^2$$
$$+ [\Delta m(V, \text{observed}) - \Delta m(V, \text{predicted})]^2$$
$$+ [\Delta m(I, \text{observed}) - \Delta m(I, \text{predicted})]^2$$

with respect to $T_h$ and $R_2$ (where the predicted amplitudes are calculated from equation 1), (iii) repeat (i) and (ii) for a range of plausible secondary star temperatures and (iv) select, from amongst the possible solutions, pairs $(R_2, T_2)$ which correspond to real stars.

Solutions for $R_2$ and the heated hemisphere temperature are plotted in Fig. 8 as a function of the secondary star temperature $T_2$. The ranges in both of the variables are surprisingly narrow. Consistency between $T_2$ and $R_2$ requires that the secondary be of spectral type close to M5, for which Reid & Hawley (2000) give a temperature of 2800 K and radius 0.2 $R_\odot$. (The radii of M4 and M6 stars are 0.26 and 0.15 $R_\odot$, respectively). The corresponding mass is 0.14 $M_\odot$.

The binary separation $A$ follows from Kepler's third law:

$$A = 4.21(M_1 + M_2)^{1/3} P^{2/3},$$

where $A$ is in solar radii, the primary and secondary masses in units of $M_\odot$ and the period $P$ in days. Substituting $P = 0.754$, $M_1 = 0.5$ and $M_2 = 0.14$, $A = 3.0\,R_\odot$ is obtained.
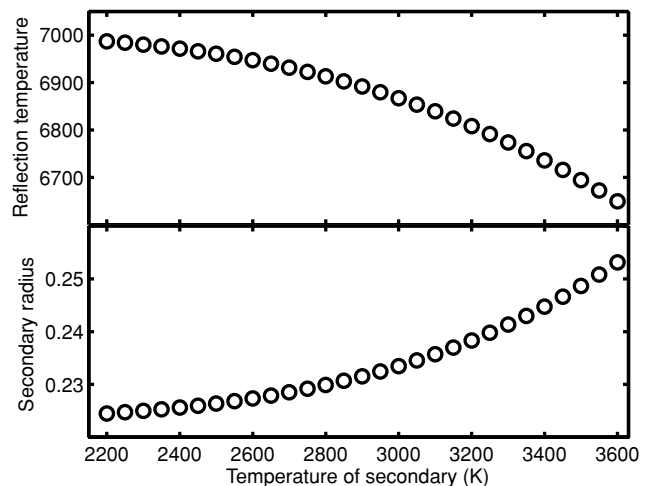


**Figure 8.** The data folded with respect to the best-fitting *I*-band period.

The mass function of the secondary star is given by Edelmann et al. (2005) as $f(M_2) = 0.0031$. With the value of $M_2$ obtained above, an inclination angle $i = 51°$ follows. As a consistency check, note that

$$\cos i > \frac{R_1 + R_2}{A} = 0.19 \,,$$

or $i < 79°$, since the system shows no eclipses.

There are currently nine sdB+M binaries known (For et al. 2008), or perhaps 10 if the very late type secondary star in HE 0230−4323 (Edelmann et al. 2005; Koen 2007) is an M dwarf (rather than being of even later spectral type). Amongst these, the 0.75-d period of JL 82 is by far the longest: next in line would be HE 0230−4323 (Edelmann et al. 2005; Koen 2007) with $P = 0.45$d. Only three other systems have periods longer than 3 h (For et al. 2008). It is thought that systems such as JL 82 will evolve into cataclysmic variables (e.g. Schreiber & Gänsicke 2003).

## ACKNOWLEDGMENTS

## REFERENCES

Baran A., Pigulski A., Koziel D., Ogloza W., Silvotti R., Zola S., 2005, MNRAS, 360, 737
Baran A., Pigulski A., O'Toole S. J., 2008, MNRAS, 385, 255
Edelmann H., 2003, PhD thesis, Univ. Erlangen-Nürnberg
Edelmann H., Heber U., Altmann M., Karl C., Lisker T., 2005, A&A, 442, 1023
Fontaine G., Green E. M., Chayer P., Brassard P., Charpinet S., Randall S. K., 2006, Balt. Astron., 15, 211
For B.-Q., Edelmann H., Green E. M., Drechsel H., Nesslinger S., Fontaine G., 2008, in Heber U., Jeffery C. S., Napiwotzki R., eds, ASP Conf. Ser. Vol. 392, Hot Subdwarfs and Related Objects. Astron. Soc. Pac., San Francisco, p. 339
Green E. M. et al., 2003, ApJ, 583, L31
Jaidee S., Lynga G., 1974, Ark. Astron., 5, 345
Kilkenny D., 2007, Commun. Asteroseismol., 150, 234
Kilkenny D., Luvhimbi E., O'Donoghue D., Stobie R. S., Koen C., Chen A., 1995, MNRAS, 276, 906
Kilkenny D., Copley C., Zietsman E., Worters H., 2007, MNRAS, 375, 1325
Koen C., 2007, MNRAS, 377, 1275
Koen C., Green E. M., 2007, MNRAS, 377, 1605
Landolt A. U., 2007, AJ, 133, 2502
Lutz R. et al., 2008, in Heber U., Jeffery C. S., Napiwotzki R., eds, ASP Conf. Ser. Vol. 392, Hot Subdwarfs and Related Objects. Astron. Soc. Pac., San Francisco, p. 339
Oreiro R., Ulla A., Pérez Hernández F., Ulla A., Garrido R., Østensen R., McDonald J., 2005, A&A, 438, 257
Randall S. K. et al., 2006a, ApJ, 633, 460
Randall S. K. et al., 2006b, ApJ, 643, 1198
Randall S. K. et al., 2006c, ApJ, 645, 1464
Reed M. D., Stiening R., 2004, PASP, 116, 506
Reed M. D. et al., 2004, ApJ, 607, 445
Reid I. N., Hawley S. L., 2000, New Light on Dark Stars. Praxis Publishing, Chichester
Schechter P. L., Mateo M., Saha A., 1993, PASP, 105, 1342
Schreiber M. R., Gänsicke B. T., 2003, A&A, 406, 305
Schuh S., Huber J., Dreizler S., Heber U., O'Toole S. J., Green E. M., Fontaine G., 2006, A&A, 445, L31
Skrutskie M. F. et al., 2006, AJ, 131, 1163
Stark M. A., Wade R. A., 2003, AJ, 126, 1455

## SUPPORTING INFORMATION

Additional Supporting Information may be found in the online version of this article:

**Figure S1.** Light curves obtained in the *V* band. The vertical width of each panel is 0.11 mag. Panels are labelled with the last two digits of the Julian day of observation.
**Figure S2.** Light curves obtained in the *I* band. The vertical width of each panel is 0.11 mag. Panels are labelled with the last two digits of the Julian day of observation.
**Figure S3.** The data folded with respect to the best-fitting *I*-band period. From top to bottom panel: *B*, *V* and *I*.

Please note: Wiley-Blackwell are not responsible for the content or functionality of any supporting materials supplied by the authors. Any queries (other than missing material) should be directed to the corresponding author for the article.

This paper has been typeset from a TeX/LaTeX file prepared by the author.